Intercombination transitions of the carbon-like isoelectronic sequence*

Liu Hao(刘 浩)[a)b)], Jiang Gang(蒋 刚)[a)†] Hu Feng(胡 峰)[c)],
Wang Chuan-Ke(王传珂)[b)], Wang Zhe-Bin(王哲斌)[b)], and Yang Jia-Min(杨家敏)[b)]

[a)] *Institute of Atomic and Molecular Physics, Sichuan University, Chengdu* 610065, *China*
[b)] *Research Center of Laser Fusion, China Academy of Engineering Physics, Mianyang* 621900, *China*
[c)] *School of Mathematic and Physical Science, Xuzhou Institution of Technoogy, Xuzhou* 221400, *China*

(Received 25 November 2012; revised manuscript received 18 December 2012)

Energy levels, wavelengths, transition rates, oscillator strengths, and lifetimes between the $2s^22p^2\ ^3P_1$, $2s^22p^2\ ^3P_2$, and $2s2p^3\ ^5S_2$ levels of ions in the carbon-like (C-like) isoelectronic sequence (nuclear charges $Z = 7$–92) are calculated in the valence and core-valence limits using the multiconfiguration Dirac–Fock method. The Breit interaction, quantum electrodynamics (QED), and finite nuclear mass effects are taken into account in subsequent relativistic configuration-interaction calculations. The calculated energies and transition rates are compared with the critically evaluated experimental values and other recent calculated results. Our calculated data are in good agreement with these data.

Keywords: carbon-like isoelectronics sequence, intercombination transition, multiconfiguration Dirac–Fock method, highly-charged ions

PACS: 32.70.Cs, 34.80.Dp, 95.30.Ky **DOI:** 10.1088/1674-1056/22/7/073202

1. Introduction

Intercombination or spin-forbidden transitions are due to the deviation from the pure LS coupling. Due to their wide existence, at least for low-Z atoms, as a consequence of the subtle relativistic spin–orbit interaction, the agreement between theoretical and experimental results is an important measure of our understanding of atomic structure and interactions. In addition, intercombination transitions are of great interest in plasma diagnostics, for example, astrophysics and tokamak studies.[1–3]

Many theoretical and experimental investigations of the spectra of carbon-like (C-like) ions have been performed previously. Träbert *et al.*[4,5] measured the level lifetime of N^+ $2s2p^3\ ^5S_2$ and transition rates of O^{2+}, F^{3+}, and S^{10+} in C-like ions by a heavy-ion storage ring, respectively. Feldman and Bhatia calculated theoretical-transition wavelengths and energy levels of Fe XXI–Kr XXXI,[6] Ne V,[7] and Ca XV[8] using the Superstructure code. Fawcett[9] presented oscillator strengths and energy levels for allowed $n = 2$–2 and $n = 2$–3 transitions in C-like ions between F IV and Ni XXIII based on calculations using the HFR code of Cowan. Zou *et al.*[10] calculated the $1s^22s^22p^2$–$1s^22s2p^3$ and $1s^2\ 2s^2\ 2p^2$–$1s^22p^4$ transitions of C-like cobalt using the relativistic configuration interaction (RCI) computation program.[11] Zhang and Sampson[12,13] used the relativistic distorted wave method to obtain values for a large number of states. Aggarwal *et al.*[14–16] obtained the rates between low-lying states for a number of ions from F IV to Ar XIII using CIV3 code. Griffin[17] and Bandnell[18] carried out a series of R-matrix close-coupling calculations of electron-impact excitations in the C-like Ne V and Fe XXI. Yuan *et al.*[19] calculated the transition probabilities of the $2s2p^3\ ^5S_2$–$2s^22p^2\ ^3P_{1,2}$ intercombination transitions in N II, and found a strong influence of relaxation effects on the transition probabilities. Fischer and Tachiev[20] calculated energy levels and transition rates for low-lying states for ions up to Al VIII using multiconfiguration Breit–Pauli wavefunctions. Energy levels, radiative transition probabilities, and autoionization rates for C-like oxygen (O^{2+}) including $1s^22s^22pnl$, $1s^22s2p^2nl$, and $1s^22p^3nl$ ($n = 2$–8, $l = 6$–$n-1$) states were calculated by Safronova *et al.*[21] with the Hartree–Fock relativistic method (Cowan code). Shen *et al.*[22] reported some transition probabilities of N II for 2p4f–2p3d and $2s2p^23d$–$2s2p^23p$ by using a semiclassical method. The wavelength and transition probabilities for electric-dipole allowed (E1) and forbidden (E2, M1, and M2) transitions among 4f and low-lying configurations for N II by using the relativistic multi-configuration Dirac–Fock (MCDF) method were also reported by Shen *et al.*[23] Transitions in C-like Xe LVI had been calculated by Aggarwal *et al.*[24] Yang *et al.*[25] performed relativistic distorted-wave calculation to determine the rate coefficients of N II in different correlation models. The theoretical energy levels, fine-structure separations, specific mass shift parameters, isotope shifts, hyperfine interaction constants, Landé gJ-factors, and transition probabilities were reported by Jönsson and Bieroń[26] for the $2s^22p^2$–$2s2p^3$ transition arrays in N II, O III, F IV, Ne V, and

*Project supported by the National Natural Science Foundation of China (Grant No. 11174213).
†Corresponding author. E-mail: gjiang@scu.edu.cn
© 2013 Chinese Physical Society and IOP Publishing Ltd

Ti XVII, using the MCDHF method. Jönsson[27] extended the work of himself and Bieroń, and researched the states of the $2s^22p^2$, $2s2p^3$, and $2p^4$ configurations for C-like ions between F IV and Ni XXIII. In their calculation, a fully relativistic GRASP code had been adopted. Zhang *et al.*[28] studied KLL dielectronic recombination (DR) processes of highly charged He-like to O-like xenon ions systematically by using MCDF method. The electric dipole (E1) oscillator strengths of lines in O III between some singlet and triplet levels had been calculated by Ateş *et al.*[29] using the weakest bound electron potential model theory and the quantum defect orbital theory. In their calculation, both multiplet and fine-structure transitions were studied. However, systematic calculations of the $2s^22p^2\ ^3P_{1,2}$–$2s2p^3\ ^5S_2$ intercombination transitions for the C-like sequence are still rarely reported, especially for from Kr^{30+} to U^{86+}. Therefore, wide ranges of transition data for C-like ions, which can provide useful parameters for the diagnosis of various plasmas, are needed.

Our calculations are motivated by the requirement of accurate fine-structure data in a variety of scientific applications, explaining the existing results and making further predictions. In this paper, we present our calculations of energy levels, wavelengths, transition rates, the oscillator strength, and the lifetime of N^+– U^{86+} in the framework of the RCI regime using MCDF wavefunctions. The Breit interaction, quantum electrodynamics (QED) and nuclear mass corrections are fully considered. At the same time, we also investigate the influence of the core-valence correlation,[30] which is rarely considered explicitly in other calculations for the C-like isoelectronic sequence.

2. Theory and method

The extended optimal level (EOL) version of the MCDF method is used to calculate the transitions. The MCDF method has been widely discussed elsewhere,[31,32] hence, we only give a brief outline in this paper.

2.1. MCDF method

In the MCDF method,[33] the configuration state functions (CSFs) are antisymmetrized linear combinations of products of Dirac spinors. A linear combination of these CSFs is then used in the construction of atomic state function (ASF) Ψ with the same J and parity P

$$\Psi(\gamma J) = \sum_r c_r \Phi_r(\gamma_r J), \tag{1}$$

where γ, required to define the CSF uniquely, can represent all properties, such as orbital occupation numbers, the coupling, seniority numbers, etc. Configuration mixing coefficients c_r are obtained through the diagonalization of the Dirac–Coulomb Hamiltonian. Configuration state functions Φ, which are eigenfunctions of J^2, J_z, and P, are constructed as linear combinations of Slater determinants. In the restricted Dirac–Fock model, Slater determinants are products of one-electron Dirac orbitals

$$\Phi(r) = \frac{1}{r}\begin{pmatrix} P_{n\kappa}(r)\chi_{\kappa m}(\hat{r}) \\ \mathrm{i}Q_{n\kappa}(r)\chi_{-\kappa m}(\hat{r}) \end{pmatrix}. \tag{2}$$

Here, n is the principal quantum number, κ and m are the relativistic angular quantum number and its z component, respectively, $\kappa = \pm(j+1/2)$ for $l = j \pm 1/2$, with l and j being the orbital and total angular momenta of the electron, $P_{n\kappa}$ and $Q_{n\kappa}$ are the large and small component one-electron radial wavefunctions, and $\chi_{\kappa m}(\hat{r})$ is the spinor spherical harmonic in the lsj coupling scheme

$$\begin{aligned}\chi_{\kappa m}(\hat{r}) &= \chi_{\kappa m}(\theta,\varphi,\sigma) \\ &= \sum_{m_s}\left\langle lm - m_s\frac{1}{2}m_s \middle| l\frac{1}{2}jm\right\rangle \\ &\quad \times Y_{lm-m_s}(\theta,\varphi)\,\xi_{m_s}(\sigma),\end{aligned} \tag{3}$$

where $\langle lm - m_s(1/2)m_s|l(1/2)jm\rangle$ is a Clebsch–Gordan coefficient, $Y_{lm-m_s}(\theta,\varphi)$ is a spherical harmonic, and $\xi_{m_s}(\sigma)$ is a spinor basis function.

The radial functions $P_{n\kappa}(r)$ and $Q_{n\kappa}(r)$ are numerically represented on a logarithmic grid and orthonormal within each κ symmetry

$$\int_0^\infty [P_{n'\kappa}(r)P_{n\kappa}(r) + Q_{n'\kappa}(r)Q_{n\kappa}(r)]\,\mathrm{d}r = \delta_{n'n}. \tag{4}$$

In the multiconfiguration self-consistent field procedure, both the radial functions and the expansion coefficients for the configuration state functions are optimized for self-consistency.

2.2. The Dirac–Coulomb Hamiltonian

All the dominant interactions in an N-electron atom or ion are included in the Dirac–Coulomb Hamiltonian

$$\hat{H}^{\mathrm{DC}} = \sum_{i=1}^{N}\hat{H}_i + \sum_{i=1}^{N-1}\sum_{j=i+1}^{N}\left|\hat{r}_i - \hat{r}_j\right|^{-1}. \tag{5}$$

The first term

$$\hat{H} = c\sum_{i=1}^{3}\left[\boldsymbol{\alpha}_i\hat{p}_i + (\beta-1)c^2 + V_{\mathrm{nuc}}(\hat{r})\right] \tag{6}$$

is the one-body contribution for an electron as its kinetic energy and interaction with the nucleus (the rest energy has been subtracted out). The nuclear potential, $V_{\mathrm{nuc}}(\hat{r})$, takes the Coulomb form $-Z/r$ (here, denotes the atomic number of the system) when nuclear volume effects are ignored. The Dirac matrices, $\boldsymbol{\alpha}_i$ and $\boldsymbol{\beta}$ in the standard representation are

$$\begin{aligned}\boldsymbol{\alpha}_i &= \begin{pmatrix} 0 & \boldsymbol{\sigma}_i \\ \boldsymbol{\sigma}_i & 0 \end{pmatrix}, \quad i = 1,2,3, \\ \boldsymbol{\beta} &= \begin{pmatrix} 1 & 0 \\ 0 & -1 \end{pmatrix},\end{aligned} \tag{7}$$

where σ_i are the usual Pauli matrices. The two-body instantaneous Coulomb interactions between the electrons contribute the second term of Eq. (5). High-order QED modifications to Eqs. (5) and (6) due to the transverse photon interaction and the QED are treated via the perturbation theory. The matrix of the Hamiltonian (5) with respect to a basis of CSFs plays a central role in all relativistic atomic structure calculations.

2.3. Relativistic configuration interaction (RCI)

RCI calculations, which use the correlated MCDF wavefunctions and include Breit interaction and quantum electrodynamic effects, can be performed when the radial orbitals are obtained. Here, only the expansions of CSFs are determined. This is achieved by digitalizing the Hamiltonian matrix. In this implementation of RCI program, an iterative Davidson method is used together with a sparse matrix representation for the large expansion.

In RCI calculations, the lowest-order correction to the Coulomb interaction between two electrons, labeled i and j, due to the exchange of a single transverse photon, is given by

$$\boldsymbol{H}_{\text{Trans}} = -\sum_{i<j}\left[\frac{\boldsymbol{\alpha}_i\cdot\boldsymbol{\alpha}_j}{R_{ij}} + (\boldsymbol{\alpha}_i\cdot\boldsymbol{\nabla}_i)(\boldsymbol{\alpha}_j\cdot\boldsymbol{\nabla}_j) \times\frac{\cos(\omega_{ij}R_{ij})}{\omega_{ij}^2 R_{ij}}\right], \tag{8}$$

where the photon frequency ω_{ij} is the difference between the diagonal Lagrange multipliers and associates with the orbitals. In general, diagonal Lagrange multipliers are approximate electron removal energies only when the orbitals are spectroscopic and singly occupied. Thus, it is difficult to know how well the code can determine the full transverse photon interaction when the correlation orbitals are present. In the long-wavelength limit ($\omega \to 0$), this reduces to the well-known Breit interaction.

2.4. Quantum electrodynamics (QED) correction

The inclusion of interactions due to fluctuations in the electron–positron and electromagnetic fields produces the radiative corrections of QED. There are two major components in the QED correction.[34]

Self-energy is the dominant QED correction to the energy which arises from the lowest-order modification to an electron's interaction with the quantized ambient electromagnetic field (including the field due to nucleus and other atomic electrons). In terms of the function $F_{n\kappa}(Z/c)$ that varies slowly with respect to its argument, the self-energy in hydrogen-like systems is given by

$$E_{n\kappa}^{\text{SE}}\left(\frac{Z}{c}\right) = \frac{Z^4}{\pi c^3 n^3} F_{n\kappa}\left(\frac{Z}{c}\right), \tag{9}$$

where tabulations of $F_{n\kappa}(Z/c)$ for the 1s, 2s, $2p_{1/2}$, and $2p_{3/2}$ states in these one-electron systems are given in Refs. [35]–[37]. In GRASPVU, a rough estimate of the self-energy is obtained by setting

$$H_{rr}^{\text{SE}} = \sum_{a=1}^{n_\omega} q_r(a)\, E_{n_a\kappa_a}^{\text{SE}},$$

$$E_{n_a\kappa_a}^{\text{SE}} = \frac{\left(Z_a^{\text{eff}}\right)^4}{\pi c^3 n^3} \times \begin{cases} F_{n_a\kappa_a}\left(\dfrac{Z_a^{\text{eff}}}{c}\right), & \text{for } 1\text{s}, 2\text{s}, 2\text{p}_{1/2}, \text{ and } 2\text{p}_{3/2} \text{ orbitals,} \\ F_{2\kappa_a}\left(\dfrac{Z_a^{\text{eff}}}{c}\right), & \text{for } n\text{s}, n\text{p}_{1/2}, \text{ and } n\text{p}_{3/2} \text{ orbitals,} \\ 0, & \text{other.} \end{cases} \tag{10}$$

The Z^{eff} that used to roughly correct for electron screening is at best an expedient intended for inner shells where the orbitals are most likely to be nearly hydrogenic. It is likely to be decreasing as n increases.

Next in order of importance is the vacuum polarization correction. To the lowest order, this is the short-range modification of the nuclear field due to screening by virtual electron-positron pairs. Expressions for the second- and fourth-order perturbation potentials that take finite nuclear size into account have been given in the literature.[38] Only diagonal contributions

$$H_{rr}^{\text{VP}} = \sum_{a=1}^{n_\omega} q_r(a) \int_0^\infty \mathrm{d}r V^{\text{VP}}(r)\left(P_{n_a\kappa_a}^2(r) + Q_{n_a\kappa_a}^2(r)\right) \tag{11}$$

from these potentials have been included in this version of GRASPVU package.

2.5. Calculation method

2.5.1. Multiconfiguration expansion

We calculate different correlation effects in a systematical manner. The correlation energy is defined as the energy difference between the exact solution of the Dirac equation and the Dirac–Fock (DF) solution. Therefore, the contribution from the correlation effect can be defined as the energy difference between the solution including the particular correlation under investigation and the DF solution. In order to classify the different kinds of correlation effects, the electrons in an atom can be divided into two types: valence electrons

and core electrons. Thus, the correlation effect between the valence electrons is defined as valence correlation (VV), and the correlation effect between the valence electrons and core electrons is defined as core-valence correlation (CV). In the MCDF approach, the correlation is represented by different constraints on the generation of the CSFs included in Eq. (1). In the VV manner, we keep core electrons fixed in all CSFs. However, in the CV manner, we allow one of the core electrons to be active to generate the CSFs.

The construction of the atomic state functions by systematical expansion of the orbitals in the active space were discussed in some earlier studies.[22,23] In our calculations, we use the active space approach to identify different configurations when we generate the CSFs. The active set is a set of orbitals including all orbitals except those common to all CSFs, and it defines the CSFs included in the ASF. In this method, the electrons from the occupied orbitals are excited to the unoccupied orbitals in the active set (AS). We increase the active space in a systematical way to make sure that the convergences of the atomic parameters are under consideration.

For C-like ions, the ground state and the first excited state configurations are $1s^2 2s^2 2p^2\ ^3P_0$ and $1s^2 2s^2 2p^2\ ^3P_1$. Consequently, we first include valance–valance correlation by keeping the core $1s^2$ closed and the same in all calculations. The AS is

$$\mathrm{AS}_1 = \{2s, 2p\}. \tag{12}$$

Then, we extend the active set as follows:

$$\mathrm{AS}_2 = \mathrm{AS}_1 + \{3s, 3p, 3d\}, \tag{13}$$

$$\mathrm{AS}_3 = \mathrm{AS}_2 + \{4s, 4p, 4d, 4f\}, \tag{14}$$

$$\mathrm{AS}_4 = \mathrm{AS}_3 + \{5s, 5p, 5d, 5f, 5g\}. \tag{15}$$

Similarly, to investigate the effect of the core-valence correlation defined above, we perform calculations including the core-valance correlation from the 1s shell, by including CSFs which only have one electron in the 1s shell.

2.5.2. Calculation process

We first generate Dirac–Fock wavefunctions in the extended optimal level (EOL) scheme for the initial doubly excited $2s^2 2p^2$ and final $2s2p^3$ configurations. In the EOL method, the radial functions and the mixing coefficients are determined by optimizing the energy functional, which is the weighted sum of the energy values corresponding to a set of $(2j+1)$ eigenstates.

We then consider limited expansions, generate CSFs from the reference configurations with relativistic subshells, and use these optimized CSFs to evaluate the transition parameters. As this procedure leads to more optimal wavefunctions than DF functions, all our investigations on the effects of correlation and higher-order corrections are carried out with respect to CSF data. Then, we expand the active space by considering the first layer of the set with $n = 3$ and $l = 0$ to two-virtual shells and optimize the orbital functions while 1s orbital is fixed. Thus, by gradually expanding the size of the active space, the convergence of the observable is obtained.

To ensure the numerical stability and reduce the processing time, during each layer by layer expansion of the virtual orbitals only the newly added orbitals are optimized while the previously generated orbitals are kept frozen. The optimized orbitals thus generated are used in the evaluation of MCDF energies and rates. In the subsequent RCI calculations, we recalculate the mixing coefficients with a frozen radial set. As the ASFs of initial and final states consisted of CSFs built from different orthonormal sets, they are first transformed to become bi-orthonormal in the transition rate calculations.

3. Results and discussion

3.1. Energy levels

The numerical values of the energy levels obtained by the MCDF method are presented in Tables 1–3, which show the energies for $2s^2 2p^2\ ^3P_{1,2}$ and $2s2p^3\ ^5S_2$ levels along C-like isoelectronic sequence up to U^{86+}. For simplicity, $1s^2$ is disregarded as every configuration contains it.

Tables 1–3 show very good agreement between our result and the past experimental data. Figure 1 shows that the MCDHF results are the most accurate. The maximum difference between the results of MCDHF and experiment is less than 1.5%, which can be understood on the basis that the MCDHF method includes a more complete treatment of relativistic effects. CV results of this work are closer to the MCDHF results, compared with the experimental results; the maximum deviation is 3%. However, the deviations of results obtained by using CIV3 and SS are up to 10% and 13%, respectively. The CIV3, and SS results are almost equal to each other. It is interesting to see how well the results from four quite different methods (MCDHF, MCDF, CIV3, and SS) agree with each other. From Fig. 1, we can see that the accuracy of our results improves with the increase of Z, and from Mn^{19+}, our method seems to produce the most accurate results available. This emphasizes that our method is credible in high-Z case. Since these four results were performed independently, it gives an extra reliability of our results.

Table 1. Energy (in cm^{-1}) for $2s^2 2p^2\ ^3P_1$ for different ions in the carbon like (C-like) isoelectronic sequence: present VV and CV calculation results, experimental and theoretical results.

Z	VV	CV	NIST[39]	MCDHF[26,27]	CIV3[15,16]	SS[6–8]	GRASP[24]
7	47	49	49	49			
8	111	114	113	114			
9	224	227	226	227	219		
10	407	412	411	411	400	416	
11	689	696	698	695	680		
12	1066	1075	1107	1112	1087		
13	1647	1658	1710	1709	1667		
14	2460	2473	2545	2540	2482		
15	3574	3590	3692	3676	3587		
16	5075	5094	5208	5203	5083		
17	7065	7087	7240	7221	7053		
18	9666	9691	9853	9854	9850		
19	13019	13048	13235	13242			
20	17287	17319	17559	17547		17663	
21	22649	22685	22959	22949			
22	29605	29647	29658	29646			
23	37806	37852	37960	37850			
24	47741	47791	47811	47788			
25	59647	59702	59850	59696			
26	73770	73831	73851	73820		73851	
27	90365	90433	90730	90415			
28	109693	109768	109770	109741		109390	
29	132024	132107	132120				
30	157634	157726	157700			157712	
31	186807	186910	186890				
32	219839	219953	219880			219896	
33	257032	257159					
34	298702	298842				298728	
35	345175	345331					
36	396790	396962	396820			396767	
37	453899	454089					
38	516869	517078	517290				
39	586080	586310					
40	661929	662182					
41	744828	745104					
42	835206	835508					
43	933509	933838					
44	1040201	1040558					
45	1155764	1156151					
46	1280699	1281105					
47	1415528	1415981					
48	1560791	1561283					
49	1717053	1717578					
50	1884897	1885461					
51	2064931	2065536					
52	2257786	2258433					
53	2464120	2464812					
54	2684612	2685350					2678069
55	2919970	2920760					
56	3170930	3171770					
57	3438260	3439150					
58	3723700	3722760					
59	4025240	4026240					
60	4346560	4347630					
63	5432740	5433990					
64	5838740	5840070					
65	6268440	6269830					
66	6722900	6724370					
67	7203280	7204830					
72	10036800	10038800					
73	10699300	10701300					
74	11397000	11399200					
76	12904700	12907100					
79	15473100	15475800					
82	18455500	18458600					
84	20702600	20706000					
85	21911000	21914500					
88	25907100	25911100					
90	28910100	28914500					
92	32214900	32219600					

Table 2. Energy (in cm^{-1}) for $2s^2 2p^2\ ^3P_2$ for different ions in the carbon like (C-like) isoelectronic sequence: present VV and CV calculation results, experimental and theoretical results.

Z	VV	CV	NIST[39]	MCDHF[26,27]	CIV3[15,16]	SS[6–8]	GRASP[24]
7	127	131	131	129			
8	301	307	306	305			
9	606	616	614	613	592		
10	1098	1112	1110	1109	1079	1139	
11	1841	1860	1859	1855	1810		
12	2887	2910	2924	2928	2952		
13	4360	4389	4420	4414	4333		
14	6342	6377	6414	6411	6303		
15	8942	8984	9045	9027	8885		
16	12280	12329	12388	12383	12202		
17	16488	16543	16629	16610	16377		
18	21702	21765	21841	21845	21839		
19	28066	28136	28225	28230			
20	35725	35801	35923	35911		36123	
21	44824	44906	45026	45030			
22	55678	55766	55730	55732			
23	68108	68201	68190	68160			
24	82416	82513	82458	82464			
25	98763	98864	98650	98806			
26	117328	117434	117354	117364		117257	
27	138310	138421	138250	138338			
28	161933	162049	161922	161951		161190	
29	188439	188561	188430				
30	218092	218222	218054			218049	
31	251172	251311	251620				
32	287973	288122	287736			287924	
33	328804	328965					
34	373986	374160				374035	
35	423851	424039					
36	478746	478950	478200			479066	
37	1053765	1054389					
38	1184407	1185082	1185600				
39	1327544	1328272					
40	1483965	1484748					
41	1654493	1655334					
42	1839984	1840886					
43	2041329	2042296					
44	2259458	2260491					
45	2495335	2496438					
46	2749963	2751118					
47	3024388	3025642					
48	3319694	3321038					
49	3637008	3638427					
50	3977504	3979010					
51	4342401	4343997					
52	4732960	4734652					
53	5150506	5152296					
54	5596396	5598290					5585471
55	6072057	6074058					
56	6578961	6581072					
57	7118646	7120874					
58	7692707	7695055					
59	8302800	8305273					
60	8950646	8953249					
63	11139005	11142027					
64	11956525	11959697					
65	12821523	12824850					
66	13736168	13739657					
67	14702753	14706409					
72	20401232	20405816					
73	21732865	21737654					
74	23135305	23140307					
76	26165492	26170941					
79	31326315	31332493					
82	37318263	37325249					
84	41832589	41840160					
85	44260088	44267966					
88	52287660	52296524					
90	58320530	58330112					
92	64959800	64970153					

Table 3. Energy (in cm^{-1}) for $2s2p^3\ ^5S_2$ for different ions in the carbon like (C-like) isoelectronic sequence: present VV and CV calculation results, experimental and theoretical results.

Z	VV	CV	NIST[39]	MCDHF[26,27]	CIV3[15,16]	SS[6–8]	GRASP[24]
7	46553	46173	46785	46480			
8	60157	59734	60325	60023			
9	74062	73594	74195	73979	71924		
10	88292	87782	88400	88177	85918	76661	
11	102918	102375	103362	102796	100334		
12	118008	117438	118100	117899	106200		
13	133740	133148	133840	133627	130817		
14	150233	149624	150770	150120	147163		
15	167652	167029	167740	167541	164416		
16	186179	185545	186251	186065	182791		
17	206021	205379	206100	205925	202457		
18	227403	226756	225918	227327	227378		
19	250575	249923	250640	250521			
20	275799	275145	275900	275770		264749	
21	303357	302702	301400	303357			
22	333800	333145	333600	333563			
23	366938	366283	366870	366700			
24	403295	402642	403268	403040			
25	443159	442508	443060	442890			
26	486807	486158	486950	486521		486955	
27	534493	533848	534760	534186			
28	586455	585813	586890	586120		585620	
29	642893	642253					
30	703989	703351				690079	
31	769884	769249					
32	840710	840075				826902	
33	916577	915942					
34	997593	996957				983898	
35	1083890	1083250					
36	1175600	1174960				1161970	
37	1272956	1272311					
38	1376188	1375538	1368900				
39	1485583	1484928					
40	1601491	1600833					
41	1724312	1723650					
42	1854471	1853805					
43	1992442	1991773					
44	2138712	2138042					
45	2293813	2293142					
46	2458279	2457606					
47	2632689	2632019					
48	2817609	2816919					
49	3013665	3013000					
50	3221471	3220810					
51	3441691	3441035					
52	3674955	3674304					
53	3922069	3921425					
54	4183613	4182977					4183779
55	4460410	4459790					
56	4753190	4752570					
57	5062790	5062180					
58	5389440	5390040					
59	5735780	5735190					
60	6100840	6100270					
63	7321670	7321140					
64	7773710	7773200					
65	8250200	8249710					
66	8752080	8751600					
67	9280660	9280200					
72	12366700	12366400					
73	13082100	13081800					
74	13833700	13833400					
76	15451800	15451600					
79	18193000	18192800					
82	21356500	21356400					
84	23730000	23730000					
85	25003100	25003100					
88	29194800	29194800					
90	32332900	32333000					
92	35774600	35774700					

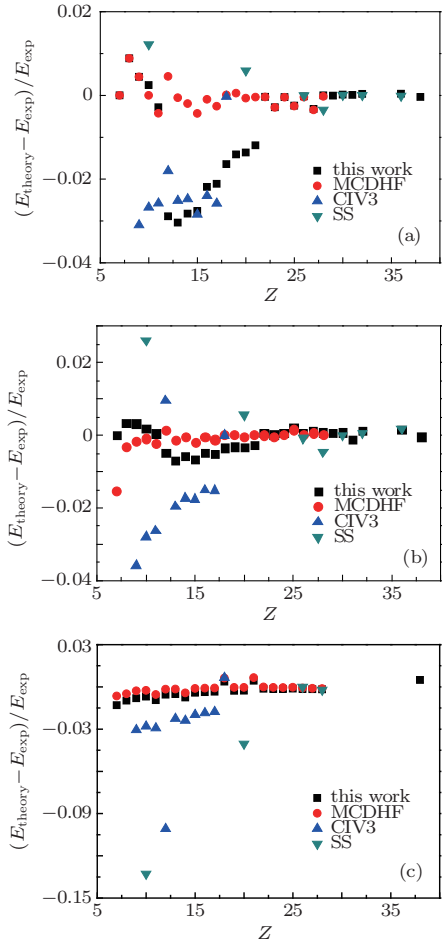


Fig. 1. (color online) Differences between the available theoretical and experimental values and our results: (a) $2s^22p^2\ ^3P_1$, (b) $2s^22p^2\ ^3P_2$, and (c) $2s2p^3\ ^5S_2$.

3.2. Wavelengths, oscillator strengths, and transition rates

Our results for wavelengths, oscillator strengths, transition rates in C-like isoelectronic sequence are presented in Tables 4 and 5 for the $2s^22p^2\ ^3P_1$– $2s2p^3\ ^5S_2$ and $2s^22p^2\ ^3P_2$–$2s2p^3\ ^5S_2$ electric dipoles (E1) transitions. In these tables, the wavelength and transition rates are tabulated for VV and CV calculations, the A-values obtained in the Babushkin (length) gauge. The oscillator strengths obtained in the Babushkin (length) and Coulomb (velocity) gauges are given. The results obtained by these two formalisms for all transitions considered in the present work coincide with each other, except for the cases of $Z = 7$–12 for which the discrepancies are larger. This can be explained easily by the fact that these transitions are affected by cancellation effects in the computation process.

Our calculated wavelengths are also compared with a few available experimental data from National Institute of Standards and Technology (NIST). Figure 2 shows the relative wavelength differences $\Delta\lambda$ between our MCDF calculations and the NIST data. It is clear that, for some transitions, these experimental data deviate from the predicted trend along the sequence. We cannot tell the difference between theoretical and experimental wavelengths? increases or decreases with Z with the help of these few data. However, we find good agreement with the NIST data, with relative differences ranging from 0% to 4.5% for these transitions.

Table 4. Wavelengths λ, transition probabilities A, and oscillator strengths f of $2s^22p^2\ ^3P_1$–$2s2p^3\ ^5S_2$.

Z	λ/nm			A/s^{-1}			f/s^{-1}		
	NIST[39]	VV	CV	NIST[39]	VV	CV	NIST[39]	S_l	S_v
7	213.9	215.0	216.8	5.15×10^{1}	4.32×10^{1}	3.09×10^{1}	5.90×10^{-8}	2.51×10^{-7}	1.63×10^{-6}
8	166.1	166.5	167.7	2.20×10^{2}	2.07×10^{2}	1.84×10^{2}	1.52×10^{-7}	3.88×10^{-7}	1.20×10^{-6}
9		135.4	136.3		7.57×10^{2}	7.11×10^{2}		9.90×10^{-7}	2.22×10^{-6}
10	113.7	113.8	114.5		2.28×10^{3}	2.20×10^{3}		2.16×10^{-6}	3.98×10^{-6}
11	98.5	97.8	98.4	5.95×10^{3}	5.98×10^{3}	5.82×10^{3}	1.41×10^{-6}	4.22×10^{-6}	6.86×10^{-6}
12	85.5	85.5	85.9		1.38×10^{4}	1.36×10^{4}		7.50×10^{-6}	1.11×10^{-5}
13	75.7	75.7	76.1	3.00×10^{4}	3.02×10^{4}	2.97×10^{4}	4.30×10^{-6}	1.29×10^{-5}	1.79×10^{-5}
14	67.5	67.7	68.0	6.19×10^{4}	6.19×10^{4}	6.10×10^{4}	7.04×10^{-6}	2.11×10^{-5}	2.79×10^{-5}
15		61.0	61.2		1.21×10^{5}	1.19×10^{5}		3.34×10^{-5}	4.25×10^{-5}
16	55.2	55.2	55.4	2.33×10^{5}	2.25×10^{5}	2.23×10^{5}	1.78×10^{-5}	5.13×10^{-5}	6.33×10^{-5}
17		50.3	50.4		4.08×10^{5}	4.03×10^{5}		7.69×10^{-5}	9.25×10^{-5}
18		45.9	46.1		7.18×10^{5}	7.10×10^{5}		1.13×10^{-4}	1.33×10^{-4}
19		42.1	42.2		1.23×10^{6}	1.22×10^{6}		1.63×10^{-4}	1.89×10^{-4}
20		38.7	38.8		2.08×10^{6}	2.07×10^{6}		2.33×10^{-4}	2.66×10^{-4}
21	35.9	35.6	35.7	3.50×10^{6}	3.46×10^{6}	3.43×10^{6}	1.10×10^{-4}	3.28×10^{-4}	3.69×10^{-4}
22	32.9	32.9	33.0	6.00×10^{6}	5.70×10^{6}	5.66×10^{6}	1.60×10^{-4}	4.60×10^{-4}	5.14×10^{-4}
23	30.4	30.4	30.5	9.10×10^{6}	9.20×10^{6}	9.13×10^{6}	2.10×10^{-4}	6.35×10^{-4}	7.02×10^{-4}
24	28.1	28.1	28.2	1.50×10^{7}	1.47×10^{7}	1.46×10^{7}	3.00×10^{-4}	8.67×10^{-4}	9.51×10^{-4}
25	26.1	26.1	26.1	2.40×10^{7}	2.31×10^{7}	2.30×10^{7}	4.10×10^{-4}	1.17×10^{-3}	1.28×10^{-3}
26	24.2	24.2	24.3	3.60×10^{7}	3.60×10^{7}	3.58×10^{7}	5.30×10^{-4}	1.58×10^{-3}	1.71×10^{-3}
27	22.5	22.5	22.6	5.60×10^{7}	5.53×10^{7}	5.50×10^{7}	7.10×10^{-4}	2.10×10^{-3}	2.26×10^{-3}
28	21.0	21.0	21.0	8.50×10^{7}	8.39×10^{7}	8.35×10^{7}	9.30×10^{-4}	2.76×10^{-3}	2.96×10^{-3}
29		19.6	19.6		1.25×10^{8}	1.25×10^{8}		3.60×10^{-3}	3.84×10^{-3}
30		18.3	18.3		1.84×10^{8}	1.84×10^{8}		4.62×10^{-3}	4.92×10^{-3}
31		17.2	17.2		2.66×10^{8}	2.65×10^{8}		5.86×10^{-3}	6.23×10^{-3}

Table 4. (*Continued*).

Z	λ/nm			A/s^{-1}			f/s^{-1}		
	NIST[39]	VV	CV	NIST[39]	VV	CV	NIST[39]	S_l	S_v
32		16.1	16.1		3.77×10^{8}	3.75×10^{8}		7.32×10^{-3}	7.75×10^{-3}
33		15.2	15.2		5.23×10^{8}	5.20×10^{8}		8.98×10^{-3}	9.49×10^{-3}
34		14.3	14.3		7.05×10^{8}	7.03×10^{8}		1.08×10^{-2}	1.14×10^{-2}
35		13.5	13.6		9.31×10^{8}	9.28×10^{8}		1.28×10^{-2}	1.35×10^{-2}
36		12.8	12.9		1.20×10^{9}	1.19×10^{9}		1.48×10^{-2}	1.56×10^{-2}
37		12.2	12.2		1.51×10^{9}	1.50×10^{9}		1.77×10^{-2}	1.68×10^{-2}
38	11.7	11.6	11.7	1.83×10^{9}	1.85×10^{9}	1.84×10^{9}	6.30×10^{-3}	1.98×10^{-2}	1.88×10^{-2}
39		11.1	11.1		2.23×10^{9}	2.22×10^{9}		2.18×10^{-2}	2.06×10^{-2}
40		10.6	10.7		2.63×10^{9}	2.62×10^{9}		2.35×10^{-2}	2.23×10^{-2}
41		10.2	10.2		3.04×10^{9}	3.03×10^{9}		2.51×10^{-2}	2.37×10^{-2}
42		9.8	9.8		3.48×10^{9}	3.46×10^{9}		2.65×10^{-2}	2.50×10^{-2}
43		9.4	9.5		3.92×10^{9}	3.90×10^{9}		2.78×10^{-2}	2.61×10^{-2}
44		9.1	9.1		4.36×10^{9}	4.34×10^{9}		2.88×10^{-2}	2.70×10^{-2}
45		8.8	8.8		4.81×10^{9}	4.79×10^{9}		2.96×10^{-2}	2.78×10^{-2}
46		8.5	8.5		5.26×10^{9}	5.23×10^{9}		3.03×10^{-2}	2.83×10^{-2}
47		8.2	8.2		5.70×10^{9}	5.68×10^{9}		3.08×10^{-2}	2.88×10^{-2}
48		8.0	8.0		6.15×10^{9}	6.12×10^{9}		3.32×10^{-2}	2.92×10^{-2}
49		7.7	7.7		6.59×10^{9}	6.57×10^{9}		3.16×10^{-2}	2.93×10^{-2}
50		7.5	7.5		7.04×10^{9}	7.01×10^{9}		3.18×10^{-2}	2.95×10^{-2}
51		7.3	7.3		7.48×10^{9}	7.45×10^{9}		3.19×10^{-2}	2.95×10^{-2}
52		7.1	7.1		7.92×10^{9}	7.89×10^{9}		3.20×10^{-2}	2.95×10^{-2}
53		6.9	6.9		8.36×10^{9}	8.33×10^{9}		3.20×10^{-2}	2.94×10^{-2}
54		6.7	6.7		8.81×10^{9}	8.77×10^{9}		3.19×10^{-2}	2.93×10^{-2}
55		6.5	6.5		9.25×10^{9}	9.21×10^{9}		2.92×10^{-2}	3.19×10^{-2}
56		6.3	6.3		9.70×10^{9}	9.66×10^{9}		2.90×10^{-2}	3.18×10^{-2}
57		6.2	6.2		1.02×10^{10}	1.01×10^{10}		2.88×10^{-2}	3.17×10^{-2}
58		6.0	6.0		1.06×10^{10}	1.06×10^{10}		2.85×10^{-2}	3.16×10^{-2}
59		5.9	5.9		1.11×10^{10}	1.10×10^{10}		2.83×10^{-2}	3.14×10^{-2}
60		5.7	5.7		1.15×10^{10}	1.15×10^{10}		2.80×10^{-2}	3.12×10^{-2}
63		5.3	5.3		1.30×10^{10}	1.29×10^{10}		2.72×10^{-2}	3.06×10^{-2}
64		5.2	5.2		1.35×10^{10}	1.34×10^{10}		2.69×10^{-2}	3.04×10^{-2}
65		5.1	5.1		1.40×10^{10}	1.39×10^{10}		2.66×10^{-2}	3.02×10^{-2}
66		4.9	4.9		1.45×10^{10}	1.44×10^{10}		2.63×10^{-2}	3.00×10^{-2}
67		4.8	4.8		1.50×10^{10}	1.49×10^{10}		2.60×10^{-2}	2.98×10^{-2}
72		4.3	4.3		1.78×10^{10}	1.77×10^{10}		2.45×10^{-2}	2.87×10^{-2}
73		4.2	4.2		1.84×10^{10}	1.83×10^{10}		2.43×10^{-2}	2.85×10^{-2}
74		4.1	4.1		1.89×10^{10}	1.90×10^{10}		2.40×10^{-2}	2.83×10^{-2}
76		3.9	3.9		2.03×10^{10}	2.02×10^{10}		2.35×10^{-2}	2.78×10^{-2}
79		3.7	3.7		2.23×10^{10}	2.22×10^{10}		2.25×10^{-2}	2.72×10^{-2}
82		3.5	3.5		2.46×10^{10}	2.43×10^{10}		2.17×10^{-2}	2.67×10^{-2}
84		3.3	3.3		2.60×10^{10}	2.58×10^{10}		2.12×10^{-2}	2.63×10^{-2}
85		3.2	3.2		2.68×10^{10}	2.66×10^{10}		2.09×10^{-2}	2.61×10^{-2}
88		3.0	3.1		2.91×10^{10}	2.89×10^{10}		2.01×10^{-2}	2.55×10^{-2}
90		2.9	2.9		3.06×10^{10}	3.05×10^{10}		1.95×10^{-2}	2.51×10^{-2}
92		2.8	2.8		3.22×10^{10}	3.20×10^{10}		1.90×10^{-2}	2.48×10^{-2}

Table 5. Wavelengths λ, transition probabilities A and oscillator strengths f of $2s^22p^2\ ^3P_2$–$2s2p^3\ ^5S_2$.

Z	λ/nm			A/s^{-1}			f/s^{-1}		
	NIST[39]	VV	CV	NIST[39]	VV	CV	NIST[39]	S_l	S_v
7	214.2	215.4	217.2	1.27×10^{2}	1.04×10^{2}	7.09×10^{1}	8.72×10^{-8}	1.09×10^{-7}	6.21×10^{-7}
8	166.6	167.1	168.3	5.48×10^{2}	5.10×10^{2}	4.46×10^{2}	2.28×10^{-7}	9.48×10^{-7}	3.16×10^{-6}
9		136.1	137.0		1.90×10^{3}	1.77×10^{3}		2.49×10^{-6}	5.87×10^{-6}
10	114.6	114.7	115.4		5.73×10^{3}	5.49×10^{3}		5.48×10^{-6}	1.05×10^{-5}
11	98.5	98.9	99.5	1.48×10^{4}	1.49×10^{4}	1.45×10^{4}	2.15×10^{-6}	1.07×10^{-5}	1.80×10^{-5}
12	86.8	86.9	87.3		3.51×10^{4}	3.43×10^{4}		1.96×10^{-5}	3.00×10^{-5}
13	77.3	77.3	77.7	7.17×10^{4}	7.45×10^{4}	7.31×10^{4}	6.42×10^{-6}	3.30×10^{-5}	4.73×10^{-5}
14	69.3	69.5	69.8	1.43×10^{5}	1.47×10^{5}	1.45×10^{5}	1.03×10^{-5}	5.29×10^{-5}	7.21×10^{-5}
15		63.0	63.3		2.75×10^{5}	2.71×10^{5}		8.12×10^{-5}	1.06×10^{-4}
16	57.5	57.5	57.7	4.91×10^{5}	4.89×10^{5}	4.82×10^{5}	2.44×10^{-5}	1.20×10^{-4}	1.53×10^{-4}
17		52.8	53.0		8.34×10^{5}	8.23×10^{5}		1.73×10^{-4}	2.14×10^{-4}
18	49.0	48.6	48.8		1.37×10^{6}	1.36×10^{6}		2.42×10^{-4}	2.93×10^{-4}
19		44.9	45.1		2.20×10^{6}	2.17×10^{6}		3.31×10^{-4}	3.93×10^{-4}
20		41.7	41.8		3.42×10^{6}	3.38×10^{6}		4.42×10^{-4}	5.18×10^{-4}
21	39.0	38.7	38.8	5.40×10^{6}	5.20×10^{6}	5.14×10^{6}	1.20×10^{-4}	5.80×10^{-4}	6.70×10^{-4}
22	36.0	36.0	36.1	8.30×10^{6}	7.72×10^{6}	7.64×10^{6}	1.60×10^{-4}	7.44×10^{-4}	8.47×10^{-4}
23	33.5	33.5	33.6	1.20×10^{7}	1.13×10^{7}	1.12×10^{7}	2.00×10^{-4}	9.45×10^{-4}	1.06×10^{-3}

Table 5. (*Continued*).

Z	λ/nm			A/s^{-1}			f/s^{-1}		
	NIST[39]	VV	CV	NIST[39]	VV	CV	NIST[39]	S_l	S_v
24	31.2	31.2	31.2	1.70×10^{7}	1.63×10^{7}	1.62×10^{7}	2.50×10^{-4}	1.18×10^{-3}	1.32×10^{-3}
25	29.0	29.0	29.1	2.50×10^{7}	2.32×10^{7}	2.30×10^{7}	3.20×10^{-4}	1.46×10^{-3}	1.62×10^{-3}
26	27.1	27.1	27.1	3.50×10^{7}	3.28×10^{7}	3.25×10^{7}	3.80×10^{-4}	1.80×10^{-3}	1.97×10^{-3}
27	25.2	25.2	25.3	4.80×10^{7}	4.58×10^{7}	4.54×10^{7}	4.60×10^{-4}	2.18×10^{-3}	2.38×10^{-3}
28	23.5	23.6	23.6	6.60×10^{7}	6.34×10^{7}	6.30×10^{7}	5.50×10^{-4}	2.63×10^{-3}	2.86×10^{-3}
29		22.0	22.0		8.72×10^{7}	8.66×10^{7}		3.15×10^{-3}	3.41×10^{-3}
30		20.6	20.6		1.19×10^{8}	1.18×10^{8}		3.76×10^{-3}	4.05×10^{-3}
31		19.3	19.3		1.60×10^{8}	1.60×10^{8}		4.46×10^{-3}	4.78×10^{-3}
32		18.1	18.1		2.14×10^{8}	2.13×10^{8}		5.24×10^{-3}	5.61×10^{-3}
33		17.0	17.0		2.83×10^{8}	2.81×10^{8}		6.12×10^{-3}	6.53×10^{-3}
34		16.0	16.1		3.68×10^{8}	3.66×10^{8}		7.07×10^{-3}	7.53×10^{-3}
35		15.2	15.2		4.71×10^{8}	4.69×10^{8}		8.09×10^{-3}	8.61×10^{-3}
36		14.4	14.4		5.94×10^{8}	5.91×10^{8}		9.15×10^{-3}	9.72×10^{-3}
37		45.6	45.9		7.36×10^{8}	7.33×10^{8}		5.2×10^{-4}	4.56×10^{-4}
38	54.6	52.1	52.5	2.00×10^{6}	1.93×10^{6}	1.87×10^{6}	1.00×10^{-4}	4.56×10^{-4}	3.87×10^{-4}
39		63.3	63.8		1.08×10^{9}	1.07×10^{9}		3.70×10^{-4}	3.06×10^{-4}
40		85.1	86.1		1.28×10^{9}	1.27×10^{9}		2.76×10^{-4}	2.16×10^{-4}
44		82.8	81.7		2.21×10^{9}	2.20×10^{9}		1.43×10^{-4}	1.77×10^{-4}
45		49.6	49.2		2.47×10^{9}	2.46×10^{9}		2.45×10^{-4}	2.75×10^{-4}
46		34.3	34.1		2.74×10^{9}	2.73×10^{9}		3.44×10^{-4}	3.69×10^{-4}
47		25.5	25.4		3.02×10^{9}	3.01×10^{9}		4.40×10^{-4}	4.61×10^{-4}
48		19.9	19.8		3.31×10^{9}	3.30×10^{9}		5.07×10^{-4}	5.51×10^{-4}
49		16.0	16.0		3.61×10^{9}	3.60×10^{9}		6.22×10^{-4}	6.36×10^{-4}
50		13.2	13.2		3.92×10^{9}	3.90×10^{9}		7.08×10^{-4}	7.19×10^{-4}
51		11.1	11.1		4.23×10^{9}	4.21×10^{9}		7.91×10^{-4}	7.99×10^{-4}
52		9.5	9.4		4.55×10^{9}	4.53×10^{9}		8.71×10^{-4}	8.77×10^{-4}
53		8.1	8.1		4.88×10^{9}	4.86×10^{9}		9.49×10^{-4}	9.51×10^{-4}
54		7.1	7.1		5.22×10^{9}	5.20×10^{9}		1.02×10^{-3}	1.02×10^{-3}
55		6.2	6.2		3.81×10^{8}	3.80×10^{8}		1.10×10^{-3}	1.09×10^{-3}
56		5.5	5.5		5.19×10^{8}	5.18×10^{8}		1.17×10^{-3}	1.16×10^{-3}
57		4.9	4.9		6.96×10^{8}	6.95×10^{8}		1.24×10^{-3}	1.23×10^{-3}
58		4.3	4.3		9.20×10^{8}	9.18×10^{8}		1.30×10^{-3}	1.29×10^{-3}
59		3.9	3.9		1.20×10^{9}	1.20×10^{9}		1.37×10^{-3}	1.36×10^{-3}
60		3.5	3.5		1.55×10^{9}	1.54×10^{9}		1.43×10^{-3}	1.42×10^{-3}
63		2.6	2.6		3.12×10^{9}	3.12×10^{9}		1.62×10^{-3}	1.60×10^{-3}
64		2.4	2.4		3.89×10^{9}	3.88×10^{9}		1.68×10^{-3}	1.66×10^{-3}
65		2.2	2.2		4.81×10^{9}	4.79×10^{9}		1.74×10^{-3}	1.72×10^{-3}
66		2.0	2.0		5.90×10^{9}	5.88×10^{9}		1.79×10^{-3}	1.77×10^{-3}
67		1.8	1.8		7.21×10^{9}	7.18×10^{9}		1.85×10^{-3}	1.83×10^{-3}
72		1.2	1.2		1.82×10^{10}	1.81×10^{10}		2.13×10^{-3}	2.10×10^{-3}
73		1.2	1.2		2.16×10^{10}	2.16×10^{10}		2.19×10^{-3}	2.16×10^{-3}
74		1.1	1.1		2.56×10^{10}	2.55×10^{10}		2.24×10^{-3}	2.21×10^{-3}
76		0.9	0.9		3.56×10^{10}	3.55×10^{10}		2.35×10^{-3}	2.32×10^{-3}
79		0.8	0.8		5.72×10^{10}	5.71×10^{10}		2.51×10^{-3}	2.48×10^{-3}
82		0.6	0.6		9.00×10^{10}	8.97×10^{10}		2.68×10^{-3}	2.64×10^{-3}
84		0.6	0.6		1.20×10^{11}	1.20×10^{11}		2.79×10^{-3}	2.75×10^{-3}
85		0.5	0.5		1.39×10^{11}	1.39×10^{11}		2.84×10^{-3}	2.80×10^{-3}
88		0.4	0.4		2.12×10^{11}	2.12×10^{11}		3.02×10^{-3}	2.97×10^{-3}
90		0.3	0.4		2.80×10^{11}	2.79×10^{11}		3.14×10^{-3}	3.09×10^{-3}
92		0.3	0.3		3.67×10^{11}	3.66×10^{11}		3.27×10^{-3}	3.22×10^{-3}

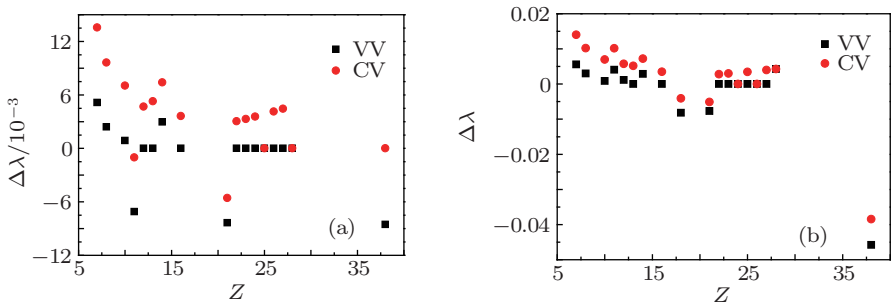


Fig. 2. (color online) The relative wavelength differences $\Delta\lambda$ between our MCDF calculations and the NIST data along the C-like isoelectronic sequence: (a) $2s^22p^2\ {}^3P_1$–$2s2p^3\ {}^5S_2$ and (b) $2s^22p^2\ {}^3P_2$–$2s2p^3\ {}^5S_2$.

3.3. Lifetimes

The radiative lifetime τ_k of an excited state k is the time during which the number of excited particles decreases to $1/e$ time ($e \approx 2.7183$) of its original value, due to spontaneous transition to low-lying states. The radiative lifetime τ_k is defined as

$$\tau_k = \left(\sum_{i \le k} A_{ik}\right)^{-1}, \tag{16}$$

where A_{ik} denotes the transition rates of all possible decay channels including forbidden and intercombination channels.

It is known that theoretical energies may not be accurate enough. Hence, theoretical emission rates increasing with ω^3 are often adjusted by replacing theoretical transition energies with empirical ones. The transition rates from $Z = 7$ to $Z = 92$ are shown in Table 6. The theory provides us the computed transition rates

$$A_1 = A(2s^2 2p^2\ ^3P_1 - 2s2p^3\ ^5S_2^0)$$

and

$$A_2 = A(2s^2 2p^2\ ^3P_2 - 2s2p^3\ ^5S_2^0),$$

while the measurable and interesting property for diagnostics is the lifetime

$$\tau = \frac{1}{A_1 + A_2}. \tag{17}$$

To some extent, the transition rates of present calculations are smaller than the accurate experimental measurements. Therefore, the lifetime obtained in our work is larger than the accurate experimental one. However, our calculated results will be closer to the experimental values with the increase of Z.

Table 6. Lifetimes (in s) for the $2s^2 2p^2\ ^3P_1$–$2s2p^3\ ^5S_2$ and $2s^2 2p^2\ ^3P_2$–$2s2p^3\ ^5S_2$ electric dipole (E1) intercombination transitions in C-like ions.

Z	A_1	A_2	$\tau_{\text{this work}}$	τ_{exp} [39]	τ_{other}
7	3.09×10^{1}	7.09×10^{1}	9.82×10^{-3}	5.60×10^{-3}	5.88×10^{-3} [4]
8	1.84×10^{2}	4.46×10^{2}	1.59×10^{-3}	1.30×10^{-3}	1.25×10^{-3} [5]
9	7.11×10^{2}	1.77×10^{3}	4.03×10^{-4}		
10	2.20×10^{3}	5.49×10^{3}	1.30×10^{-4}		
11	5.82×10^{3}	1.45×10^{4}	4.92×10^{-5}	4.82×10^{-5}	
12	1.36×10^{4}	3.43×10^{4}	2.09×10^{-5}		
13	2.97×10^{4}	7.31×10^{4}	9.73×10^{-6}	9.83×10^{-6}	
14	6.10×10^{4}	1.45×10^{5}	4.85×10^{-6}	4.88×10^{-6}	
15	1.19×10^{5}	2.71×10^{5}	2.56×10^{-6}		
16	2.23×10^{5}	4.82×10^{5}	1.42×10^{-6}	1.38×10^{-6}	
17	4.03×10^{5}	8.23×10^{5}	8.16×10^{-7}		
18	7.10×10^{5}	1.36×10^{6}	4.83×10^{-7}		
19	1.22×10^{6}	2.17×10^{6}	2.95×10^{-7}		
20	2.07×10^{6}	3.38×10^{6}	1.83×10^{-7}		
21	3.43×10^{6}	5.14×10^{6}	1.17×10^{-7}	1.12×10^{-7}	
22	5.66×10^{6}	7.64×10^{6}	7.52×10^{-8}	6.99×10^{-8}	
23	9.13×10^{6}	1.12×10^{7}	4.92×10^{-8}	4.74×10^{-8}	
24	1.46×10^{7}	1.62×10^{7}	3.25×10^{-8}	3.13×10^{-8}	
25	2.30×10^{7}	2.30×10^{7}	2.17×10^{-8}	2.04×10^{-8}	
26	3.58×10^{7}	3.25×10^{7}	1.46×10^{-8}	1.41×10^{-8}	
27	5.50×10^{7}	4.54×10^{7}	9.96×10^{-9}	9.62×10^{-9}	
28	8.35×10^{7}	6.30×10^{7}	6.83×10^{-9}	6.62×10^{-9}	
29	1.25×10^{8}	8.66×10^{7}	4.73×10^{-9}		
30	1.84×10^{8}	1.18×10^{8}	3.31×10^{-9}		
31	2.65×10^{8}	1.60×10^{8}	2.35×10^{-9}		
32	3.75×10^{8}	2.13×10^{8}	1.70×10^{-9}		
33	5.20×10^{8}	2.81×10^{8}	1.25×10^{-9}		
34	7.03×10^{8}	3.66×10^{8}	9.35×10^{-10}		
35	9.28×10^{8}	4.69×10^{8}	7.16×10^{-10}		
36	1.19×10^{9}	5.91×10^{8}	5.61×10^{-10}		
37	1.50×10^{9}	7.33×10^{8}	4.48×10^{-10}		
38	1.84×10^{9}	1.87×10^{6}	5.43×10^{-10}	5.46×10^{-10}	
39	2.22×10^{9}	1.07×10^{9}	3.04×10^{-10}		
40	2.62×10^{9}	1.27×10^{9}	2.57×10^{-10}		
41	3.03×10^{9}	1.48×10^{9}	2.22×10^{-10}		
42	3.46×10^{9}	1.71×10^{9}	1.93×10^{-10}		
43	3.90×10^{9}	1.95×10^{9}	1.71×10^{-10}		
44	4.34×10^{9}	2.20×10^{9}	1.53×10^{-10}		
45	4.79×10^{9}	2.46×10^{9}	1.38×10^{-10}		
46	5.23×10^{9}	2.73×10^{9}	1.26×10^{-10}		
47	5.68×10^{9}	3.01×10^{9}	1.15×10^{-10}		
48	6.12×10^{9}	3.30×10^{9}	1.06×10^{-10}		
49	6.57×10^{9}	3.60×10^{9}	9.83×10^{-11}		
50	7.01×10^{9}	3.90×10^{9}	9.17×10^{-11}		
51	7.45×10^{9}	4.21×10^{9}	8.58×10^{-11}		
52	7.89×10^{9}	4.53×10^{9}	8.05×10^{-11}		
53	8.33×10^{9}	4.86×10^{9}	7.58×10^{-11}		
54	8.77×10^{9}	5.20×10^{9}	7.16×10^{-11}		7.01×10^{-11} [24]
55	9.21×10^{9}	3.80×10^{8}	1.04×10^{-10}		
56	9.66×10^{9}	5.18×10^{8}	9.83×10^{-11}		
57	1.01×10^{10}	6.95×10^{8}	9.26×10^{-11}		
58	1.06×10^{10}	9.18×10^{8}	8.68×10^{-11}		
59	1.10×10^{10}	1.20×10^{9}	8.20×10^{-11}		
60	1.15×10^{10}	1.54×10^{9}	7.67×10^{-11}		
63	1.29×10^{10}	3.12×10^{9}	6.24×10^{-11}		
64	1.34×10^{10}	3.88×10^{9}	5.79×10^{-11}		
65	1.39×10^{10}	4.79×10^{9}	5.35×10^{-11}		
66	1.44×10^{10}	5.88×10^{9}	4.93×10^{-11}		
67	1.49×10^{10}	7.18×10^{9}	4.53×10^{-11}		
72	1.77×10^{10}	1.81×10^{10}	2.79×10^{-11}		
73	1.83×10^{10}	2.16×10^{10}	2.51×10^{-11}		
74	1.90×10^{10}	2.55×10^{10}	2.25×10^{-11}		
76	2.02×10^{10}	3.55×10^{10}	1.80×10^{-11}		
79	2.22×10^{10}	5.71×10^{10}	1.26×10^{-11}		
82	2.43×10^{10}	8.97×10^{10}	8.77×10^{-12}		
84	2.58×10^{10}	1.20×10^{11}	6.86×10^{-12}		
85	2.66×10^{10}	1.39×10^{11}	6.04×10^{-12}		
88	2.89×10^{10}	2.12×10^{11}	4.15×10^{-12}		
90	3.05×10^{10}	2.79×10^{11}	3.23×10^{-12}		
92	3.20×10^{10}	3.66×10^{11}	2.51×10^{-12}		

4. Conclusion

We have performed systematical MCDF and RCI calculations of $2s^2 2p^2\ ^3P_{1,2}$–$2s2p^3\ ^5S_2$ intercombination transition parameters in the C-like isoelectronic sequence (from $Z = 7$ to $Z = 92$). Optimal orbital sets were used for the initial- and final-state functions. The calculations take valence and core-

valence correlations into account by configuration expansions based on orbital sets with principal quantum numbers $n = 3$, 4, and 5 and quantum numbers $l = 0$, 1, 2, 3, 4, and 5. Our results for the energies, wavelengths, and transition rates are compared with the earlier available data. The transition wavelengths of the C-like ions carried out in this work are in good agreement with the available experimental and theoretical results. Since a large number of CSFs have been generated, the Breit interaction and QED have been considered in this calculation. We believe that these results will be useful in analyzing the existing experimental data and planning new experiments. It is also clear that these kinds of transitions need further work, especially experimental work, to distinguish different calculation methods and devote their usages to plasma diagnostics.

Acknowledgment

The authors are grateful to Fischer C F for providing the GRASPVU package for free and extend their appreciation to the staff at the Research Center of Laser Fusion, CAEP, for helping with these calculations.

References

[1] Ellis D G, Martinson I and Träbert E 1990 *Comm. At. Mol. Phys.* **22** 241
[2] Abdallah J, Faenov A Y, Hammer D, Pikuz S A, Csanak G and Clark R E H 1996 *Phys. Scr.* **53** 705
[3] Bhatia A K and Doschek G A 1993 *At. Data Nucl. Data Tables* **55** 315
[4] Träbert E, Wolf A, Pinnington E H, Linkemann J, Knystautas E J, Curtis A, Bhattacharya N and Berry H G 1998 *Phys. Rev. A* **58** 4449
[5] Träbert E, Calamai A G, Gillaspy J D, Gwinner G, Tordoir X and Wolf A 2000 *Phys. Rev. A* **62** 022507
[6] Feldman U and Seely J F 1985 *At. Data Nucl. Data Tables* **32** 305
[7] Bhatia A K and Doschek G A 1993 *At. Data Nucl. Data Tables* **55** 315
[8] Bhatia A K and Doschek G A 1993 *At. Data Nucl. Data Tables* **53** 195
[9] Fawcett B C 1987 *At. Data Nucl. Data Tables* **37** 367
[10] Zou Y and Li J M 1990 *Chin. Phys. Lett.* **7** 216
[11] Zhao Z X and Li J M 1985 *Acta Phys. Sin.* **34** 1469 (in Chinese)
[12] Zhang H L and Sampson D H 1996 *At. Data Nucl. Data Tables* **63** 275
[13] Zhang H L and Sampson D H 1997 *At. Data Nucl. Data Tables* **65** 183
[14] Aggarwal K M, Hibbert A and Keenan F P 1997 *Astrophys. J. Suppl. Ser.* **108** 393
[15] Aggarwal K M 1998 *Astrophys. J. Suppl. Ser.* **118** 589
[16] Aggarwal K M, Keenan F P and Msezane A Z 2001 *Astrophys. J. Suppl. Ser.* **136** 763
[17] Griffin D C and Badnell N R 2000 *J. Phys. B: At. Mol. Opt. Phys.* **33** 4389
[18] Badnell N R and Griffin D C 2001 *J. Phys. B: At. Mol. Opt. Phys.* **34** 681
[19] Yuan P, Liu X S, Xie L Y, Zhang Y J and Dong C Z 2003 *Chin. Phys.* **12** 271
[20] Fischer C F and Tachiev G 2004 *At. Data Nucl. Data Tables* **87** 1
[21] Safronova U I, Ralchenko Y, Murakami I, Kato T and Kato D 2006 *Phys. Scr.* **73** 143
[22] Shen X Z, Yuan P, Zhang H M and Wang J 2007 *Chin. Phys.* **16** 2935
[23] Shen X Z, Yuan P and Liu J 2010 *Chin. Phys. B* **19** 053101
[24] Aggarwal K M, Keenan F P and Lawson K D 2010 *At. Data Nucl. Data Tables* **96** 123
[25] Yang N X, Dong C Z, Jiang J and Xie L Y 2010 *Chin. Phys. B* **19** 093101
[26] Jönsson P and Bieroń J 2010 *J. Phys. B: At. Mol. Opt. Phys.* **43** 074023
[27] Jönsson P, Rynkun P and Gaigalas G 2011 *At. Data Nucl. Data Tables* **97** 648
[28] Zhang D H, Shi Y L, Jiang J, Dong C Z and Koike F 2012 *Chin. Phys. B* **21** 013402
[29] Ateş Ş Çelik G, Tekeli G and Taşer M 2012 *At. Data Nucl. Data Tables* **98** 1
[30] Hu F, Yang J M, Wang C K, Zhang J Y, Jiang G and Zhu Z H 2011 *Acta Phys. Sin.* **60** 103104 (in Chinese)
[31] Hao L H, G Jiang, Song S Q, and Hu F 2008 *At. Data Nucl. Data Tables* **94** 739
[32] Hu F, Yang J M, Wang C K, Jing L F, Chen S B, Jiang G, Liu H, and Hao L H 2011 *Phys. Rev. A* **84** 042506
[33] Song S Q and Peng F 2006 *J. Phys. B: At. Mol. Opt. Phys.* **39** 2087
[34] Kim Y K, Baik D H, and Indelicato P 1991 *Phys. Rev. A* **44** 148
[35] Mohr P J 1975 *Phys. Rev. Lett.* **34** 1050
[36] Mohr P J 1982 *Phys. Rev. A* **26** 2338
[37] Johnson W R and Soff G 1985 *At. Data. Nucl. Data Tables* **33** 405
[38] Fullerton L W and Rinker Jr G A 1976 *Phys. Rev. A* **13** 1283
[39] Kramida A, Ralchenko Y, Reader J and NIST ASD Team 2012 http://physics.nist.gov/asd